Published in final edited form as:
Eur J Nucl Med Mol Imaging. 2007 August ; 34(8): 1291–1301. doi:10.1007/s00259-006-0280-6.

The use of ^{18}F-fluoride and ^{18}F-FDG PET scans to assess fracture healing in a rat femur model

W. K. Hsu, **B. T. Feeley**, **L. Krenek**, **D. B. Stout**, and **A. F. Chatziioannou**
Department of Orthopaedic Surgery, David Geffen School of Medicine at UCLA, Center for Health Sciences, 76-134, 10833 LeConte Avenue, Los Angeles, CA 90095, USA

J. R. Lieberman
The Musculoskeletal Institute, Department of Orthopaedic Surgery, University of Connecticut Health Center, 263 Farmington Avenue, Farmington, CT 06030-5456, USA

Abstract

Purpose—Currently available diagnostic techniques can be unreliable in the diagnosis of delayed fracture healing in certain clinical situations, which can lead to increased complication rates and costs to the health care system. This study sought to determine the utility of positron emission tomography (PET) scanning with ^{18}F-fluoride ion, which localizes in regions of high osteoblastic activity, and ^{18}F-fluorodeoxyglucose (FDG), an indicator of cellular glucose metabolism, in assessing bone healing in a rat femur fracture model.

Methods—Fractures were created in the femurs of immuno-competent rats. Animals in group I had a fracture produced via a manual three-point bending technique. Group II animals underwent a femoral osteotomy with placement of a 2-mm silastic spacer at the fracture site. Fracture healing was assessed with plain radiographs, ^{18}F-fluoride, and ^{18}F-FDG PET scans at 1, 2, 3, and 4-week time points after surgery. Femoral specimens were harvested for histologic analysis and manual testing of torsional and bending strength 4 weeks after surgery.

Results—All fractures in group I revealed abundant callus formation and bone healing, while none of the nonunion femurs were healed via assessment with manual palpation, radiographic, and histologic evaluation at the 4-week time point. ^{18}F-fluoride PET images of group I femurs at successive 1-week intervals revealed progressively increased signal uptake at the union site during fracture repair. In contrast, minimal tracer uptake was seen at the fracture sites in group II at all time points after surgery. Data analysis revealed statistically significant differences in mean signal intensity between groups I and II at each weekly interval. No significant differences between the two groups were seen using ^{18}F-FDG PET imaging at any time point.

Conclusion—This study suggests that ^{18}F-fluoride PET imaging, which is an indicator of osteoblastic activity in vivo, can identify fracture nonunions at an early time point and may have a role in the assessment of longitudinal fracture healing. PET scans using ^{18}F-FDG were not helpful in differentiating metabolic activity between successful and delayed bone healing.

Keywords

^{18}F-FDG; Positron emission tomography; Bone; ^{18}F-fluoride ion; Fracture nonunion

jlieberman@uchc.edu .

Introduction

Every year approximately 5% of all long bone fractures in the United States suffer delayed healing [1]. Multiple factors contribute to the development of delayed fracture healing, including extensive bone loss or soft tissue damage, compromised vascular supply, and poor fracture fixation [2-4]. Clinical outcomes of fracture nonunions can be potentially devastating, requiring multiple surgical procedures, high morbidity, and frequent follow-up office visits.

Lower extremity nonunions have a significant negative impact on quality of life [5]. Fracture nonunions and delayed unions are associated with disability, pain, and prolonged rehabilitation periods. Furthermore, even 3 years after the successful treatment of a nonunion, Short Form-36 scores, which measure general physical, mental, and emotional well-being, are significantly lower than in age-matched controls [6]. Patients with nonunions of the lower extremities also report significantly lower physical and mental health scores when compared to those with rheumatoid arthritis and osteoarthritis of the knee, hip, or shoulder [5].

Delays in fracture healing are associated with a significant increase in health care costs [7-9]. In a comparison of early versus delayed operative treatment of tibial shaft fractures (within 12 h and longer than 12 h, respectively), a cost-effectiveness analysis revealed costs of $7,330 per patient and $458 (both in Canadian dollars) for each week of delayed fracture healing in the latter group [7]. Similarly, Heckman and Sarasohn-Kahn reported significant cost savings to third-party payors and employers with reduced healing time of tibia fractures [9]. Clearly, fracture nonunions and delayed unions are a major burden on health care systems worldwide.

A number of imaging modalities are commonly used in the assessment of fracture healing. Traditionally, plain radiographs have been utilized to serially follow callus formation. But in many clinical situations, it is often difficult to determine when a fracture has actually healed on uniplanar views, especially with hardware in place. The use of computed tomography (CT) scanning technology improves anatomical visualization by offering three-dimensional reconstructions of bony architecture and has contributed to the assessment of healing in certain fractures [10-15]. However, CT scans and plain radiographs detect mineralized bone formation, which is the late manifestation of the fracture healing process. Moreover, CT scans demonstrate low specificity in the diagnosis of fracture nonunions in long bones [15,16]. The use of ultrasound technology has also been studied in the evaluation of bony healing in certain fractures [17-21], but because surgeons typically do not have experience evaluating ultrasound images, it has not been routinely used in the diagnosis of delayed fracture healing.

Magnetic resonance imaging (MRI) is a valuable diagnostic tool, utilizing a variation of different signal intensities to identify soft tissues and bone. However, despite its use for the diagnosis of carpal bone nonunions and spinal pseudarthroses [22-25], MRI has not been useful in evaluating delayed fracture healing in the long bones. Scintigraphic studies with ^{99m}Tc-labeled compounds have also been used to evaluate carpal bones [26,27]; however, multiple studies have demonstrated no significant differences in tracer uptake between tibia fractures that heal normally and those that form nonunions [28,29].

None of the imaging modalities available have been shown to aid in the early prediction or diagnosis of delayed healing in a long bone fracture nonunion. Furthermore, these imaging methods provide no details related to the biologic potential of the fracture site. Current diagnostic protocols for fracture healing commonly recommend serial plain radiographs to assess interval callus formation at either weekly or monthly intervals and CT scans for

equivocal findings during the late stages of fracture healing [15]. Consequently, in many challenging clinical situations, surgeons may wait 9 months to a year before formally diagnosing a nonunion because of the limitations of current imaging tools. Surgeons then postpone treatment decisions because of the problems in assessing fracture repair [30]. For this reason, surgical intervention for nonunions may be unnecessarily delayed, leading to poorer outcomes [7,9].

Positron emission tomography (PET) scanning demonstrates localized metabolic activity with the uptake of radioactive isotopes in tissue [31]. PET imaging has historically been used to characterize malignant and benign tumors, and recent studies have utilized PET technologies with novel tracers to measure skeletal metabolic activity. ^{18}F-fluoride ion, a positron-emitting isotope, has been shown to deposit preferentially at the surface of bone, where the greatest activity of remodeling and turnover are seen [32,33]. ^{18}F-fluoride ion exchanges with hydroxyl groups on hydroxyapatite to form fluoroapatite, which subsequently incorporates into the formation of bone matrix [33,34]. The uptake of ^{18}F-fluoride tracer correlates with skeletal blood flow and has been shown to exhibit superior pharmacokinetic properties compared to ^{99m}Tc-labeled biphosphonates [35-40]. While metabolic activity quantification methods using ^{99m}Tc-labeled compounds have been unsuccessful [41], recent uses of ^{18}F-fluoride ion include the measurement of regional bone metabolism in metastatic musculoskeletal tumors, osteoporosis, and Paget's disease [42-45].

^{18}F-fluorodeoxyglucose (FDG) has classically been used in PET imaging as a screening tool in characterizing the spread of malignant tumors [46]. Uptake of ^{18}F-FDG is seen in areas of increased cellular glucose metabolism and serves as a marker for localized metabolic activity. It has been used to assess musculoskeletal tumors, joint arthroplasty loosening, and osteoblastic metastases from prostate cancer [47-55].

The use of PET scanning as a diagnostic tool for fracture nonunions is attractive because it can provide a direct quantitative assessment of metabolic activity in a region of interest in a noninvasive manner. Because objective evaluation and prediction of fracture healing can be challenging with current diagnostic tools, it has been hypothesized that a PET scan could be used to quantify bone formation longitudinally during bone repair [56]. Existing imaging methods yield little information regarding the biologic activity of the fracture site, especially during the chronologic stages of healing, and surgeons often delay surgical interventions until they are sure that a fracture will not heal.

Since ^{18}F-fluoride ion has been shown to measure local osteoblastic activity and correlate with bone histomorphometry indices of bone formation [57,58], its use could provide valuable initial information in the treatment decisions for delayed fracture healing. Furthermore, PET scans using ^{18}F-FDG could reveal the metabolic activity of the soft tissue adjacent to a fracture site. An imaging technique that could assess the biologic behavior and predict the formation of a nonunion at an early time point after the fracture could lead to earlier surgical intervention, more rapid fracture healing, and decreased costs to the health care system. To date, the role of PET imaging in the assessment of fracture healing has not been elucidated. The aim of this study was to assess the utility of PET scan in the assessment of fracture healing in a rat femur model.

Materials and methods

Intramedullary fixation was used for rat femurs in two study groups. In group I animals, standard femoral fractures were created using a manual three-point bending technique. In group II, a spacer was placed at the fracture site to interfere with direct bony apposition for the length of the study. Animals then underwent comparison plain radiographs and PET

scans on a weekly basis to follow fracture healing. A total of 14 6- to 10-month-old Lewis rats were used, and seven femurs were evaluated in each study group. All animal procedures were performed with the approval of the UCLA Chancellor's Animal Research Committee (ARC). Animals were housed in accordance with the UCLA Department of Laboratory Animal Medicine guidelines, and were provided with food and water ad libitum.

Operative protocol

Gas anesthesia was administered using inhalational 1–2% isoflurane and oxygen throughout the procedure. Animals were prepped and draped in standard fashion. For animals in both group I and group II, a 5-mm incision was made medial to the patella for access to the knee joint. A 4-mm parapatellar arthrotomy was performed to expose the femoral condyles. An 18-gauge needle was introduced into the distal femur in a retrograde fashion, advanced through the intramedullary canal, and seated proximally into the trochanteric region. A second 4-mm incision was made over the mid-diaphyseal region. The quadriceps muscles were bluntly dissected away from the femur and care was taken to leave the periosteum intact. For the group I animals, a femoral fracture was created via a manual three-point bending technique. In group II animals, an osteotomy site was created in the femoral shaft using a 3-mm drill with a carbide burr. A 2-mm silastic spacer was then placed and secured with a 4–0 Vicryl suture, ensuring interruption of bony end contact. The muscle fascia and arthrotomy were closed with interrupted 4–0 Vicryl suture. The skin was closed in a separate layer with interrupted 4–0 Vicryl suture. Animals were subsequently placed in a recovery chamber at room temperature and monitored for weight bearing. Pain medicine was administered intramuscularly as needed in the first 48 h postoperatively.

Radiographic analysis and manual palpation

At weekly intervals until sacrifice at 4 weeks, animals from each treatment group were anesthetized and radiographs were obtained using a Faxitron (Field Emission Corp., McMinniville, OR). Using the 4-week radiograph, two blinded independent observers examined and scored the amount of visible bone formation within the fracture site using a previously described method [59]. A graded scoring system (0, minimal to no evidence of new bone formation; 1, evidence of bone formation, complete healing questionable; 2, solid-appearing bone, complete healing) was used by each observer to grade each femur. At the time of sacrifice, the presence or absence of a solid union was confirmed by manual palpation by two blinded reviewers. The femur was tested manually for torsional and bending strength and compared to the untreated, intact femurs. A graded scoring system (0, no evidence of bony union; 1, complete bony union questionable; 2, complete bony healing) was used to grade each specimen. Individual scores from the reviewers were then added together to obtain the final score (0–4). Final scores were then averaged in each group, and error bars were calculated. Any femurs displaying characteristics of an incomplete union were considered to be a nonunion. A κ statistic was calculated as a measure of interobserver reliability for the blinded independent observers.

Tracer preparation

Fluoride ion was produced using ^{18}O-labeled water and proton bombardment using a RDS cyclotron (CTI, Knoxville, TN). ^{18}F-fluoride ion was formed at specific activities of approximately 1,000 Ci/mmol using a method reported by Wieland et al. [60]. ^{18}F-fluorodeoxyglucose [also known as (2-deoxy-2[^{18}F]fluoro-D-glucose) or FDG] was synthesized by the method described by Hamacher et al. [61] at specific activities of approximately 1.85×10^5 MBq/mmol.

PET scan imaging protocol

Using an ARC-approved calibrated imaging chamber, which provided anesthesia with the continuous delivery of 1–3% isoflurane in oxygen and temperature control at 36°C [62], all animals underwent PET scans at weekly intervals after surgery until time of sacrifice. Rats were directly injected with approximately 74 MBq of ^{18}F-fluoride ion via the tail vein using a tuberculin syringe, and maintained under gas anesthesia in either a heated induction chamber or the microPET bed system during tracer uptake. Bladders were manually expressed 5 min prior to imaging to decrease background signal. Animals were secured in the prone position using an aluminum mounting plate on the imaging chamber, with bilateral femurs positioned perpendicular to the camera axis. Lower extremity images with a 15-min acquisition time were obtained by a microPET FOCUS 220 system [63] (CTI Concorde Microsystems LLC, Knoxville TN, USA) 1 h after radioactive tracer injection. Animals were then placed in a recovery chamber and monitored carefully for respiratory difficulties. PET scan images were reconstructed using filtered backprojection and an iterative three-dimensional reconstruction technique (MAP) [64]. Filtered backprojection images were used for quantitation of tracer uptake. Lower extremity scans using the same acquisition protocol with 74 MBq of ^{18}F-FDG were performed for all rats in both treatment groups at the same weekly intervals.

Quantitative analysis

PET scan data were analysed and quantified by AMIDE (A Medical Image Data Examiner) version 0.7.15 [65]. Plain anteroposterior radiographs were superimposed on reconstructed PET images and fracture sites were identified and marked for each scan. Regions of interest (ROIs) in a box configuration measuring 2 mm×4 mm were then drawn on coronal images encompassing the fracture site (Fig. 1). ROIs were then applied to several successive planes measuring 4 mm in depth. The size of the ROI was standardized to approximate the actual size of the femoral defect seen on plain radiographic images. Mean signal intensity (MBq/cc) within the volumes of interest was calculated using the AMIDE data analysis tool. Values were then corrected for rat weight and actual tracer dose injected. Data were reported as standardized uptake value (SUV) and evaluated by two blinded reviewers. Data points at weekly time points were compiled and analyzed.

Histologic analysis

Following sacrifice, femurs from the nonunion and standard fracture groups were subjected to histologic analysis. The quadriceps and hamstring muscles were removed and specimens were fixed in 40% ethanol at 4°C. After dehydration and cleaning, the 18-gauge needle was removed and the specimens were embedded in polymethyl-methacrylate. Serial cross-sections of 200 μm thickness were cut in a longitudinal fashion from the central 5 mm of the femur, mounted on plastic slides, and ground to a thickness of 100 μm. The samples were then polished and stained with toluidine blue, which is routinely used to demonstrate the presence of undecalcified mineralized bone in histologic sections.

Statistical analysis

For each experiment, data was reported as a mean ± standard deviation. The radiographic findings and manual palpation scores were compared with a nonparametric Kruskal-Wallis test comparing the distributions of ranked data in the two groups. Data obtained from ROI calculations were compared using two-way analysis of variance. A κ statistic was calculated as a measure of interobserver reliability for the two blinded independent observers. Statistical significance was considered present when the p value was less than 0.05.

Results

Plain radiographs and PET scans from group I, treated with three-point bending, and group II animals, treated with a silastic spacer, were evaluated at weekly intervals. Review of rat femurs at the 4-week time point via manual palpation (score=4.0±0.0) and plain radiographs (score=3.7±0.3) confirmed bony healing of all femurs in group I (8/8). In group II femurs, the absence of bridging bone was also confirmed in all eight specimens (manual palpation score=0, radiographic score=0.4±0.3). There was consistent agreement among the reviewers for both manual palpation (κ=1.00) and radiographic evaluation (κ=0.96).

Histologic analysis of the femurs in group I 4 weeks after surgery revealed newly formed bridging trabecular bone along both cortices, consistent with healing of the fractures. In contrast, all femurs in group II were noted to have a nonunion, with fibrous tissue present at the bone defect site (Fig. 2).

Radioactive tracer uptake measured from ^{18}F-fluoride PET scans of animals in groups I and II at the 1, 2, 3, and 4-week time points was quantified and analyzed, showing unequivocal differences between the treatment groups (Fig. 3). A statistically significantly higher SUV was evident in group I femurs when compared to group II femurs at all time points ($p \leq 0.005$). A progressive increase in net uptake in ^{18}F-fluoride ion at the surgical site was seen in group I femurs between the 1- and 3-week time points. The SUV was statistically significantly higher at the 3- and 4-week time points than at the 1-week time point ($p \leq 0.01$). SUV remained high at the 4-week time point, even after substantial bony healing was seen on plain radiographs. Conversely, in group II, the femurs exhibited significantly lower levels of ^{18}F-fluoride ion net uptake at all time points ($p \leq 0.005$). Furthermore, a decline in signal intensity was seen after week 2, but this was not found to be statistically significant. There was minimal variability among group II femurs, with SUV measured below 1.0 for all specimens (Fig. 3).

SUVs measured from PET scan images obtained with ^{18}F-FDG uptake revealed variable results in both groups at all time points (Fig. 4). Although signal intensities in ROIs increased minimally at weekly intervals in both group I and group II, there were no statistically significant differences either between the groups at any time point (*p* values 0.10–0.92) or among time points within each group.

PET images of the group I femurs using ^{18}F-fluoride ion were compared to plain anteroposterior radiographs at weekly intervals (Fig. 5). Assessment of plain radiographs of the femurs did not reveal discernible callus formation around the fracture site until 2 weeks after surgery. Progressive new bone formation was seen each week thereafter until all of the femurs were healed radiographically at the 4-week time point. Evaluation of the corresponding ^{18}F-fluoride ion PET scan images revealed discernible tracer uptake as early as 1 week after surgery with increasing signal intensity at successive 1-week intervals. At the 4-week time point, a large localized region of intense ^{18}F-fluoride ion uptake representing osteoblastic activity was seen at the fracture site. PET images of fractures at the 3- and 4-week time points showed markedly increased tracer uptake at the fracture site when compared to earlier stages of fracture healing (Fig. 5). Longitudinal assessment of fracture healing using PET images revealed more obvious differences between time points than those found from plain radiographs, which showed relatively subtle changes. In contrast, evaluation of corresponding PET images using ^{18}F-FDG at all time points revealed localized tracer uptake that did not correlate with radiographic bony healing (Fig. 5).

Evaluation of the plain radiographs and corresponding PET scan and histologic images of group II femurs revealed no healing of the fracture and minimal biologic activity (Fig. 6). Plain AP radiographs of femoral specimens showed a gap in the mid-diaphyseal region,

which was present 1 week after surgery and at successive weekly intervals thereafter. Although tracer uptake was seen at the proximal and distal bony ends of the fracture site, ^{18}F-fluoride ion PET scan images demonstrated significantly lower mean signal intensity at all time points, in comparison to those from group I (Fig. 3). A lower localized signal uptake could also be visualized at all weekly time points on reconstructed images (Fig. 6). Furthermore, signal intensity measurements were statistically significantly different between the groups at the 1, 2, 3, and 4-week time points (Fig. 3). Similar to those in group I, PET images using ^{18}F-FDG in group II animals demonstrated localized tracer uptake within the nonunion site despite the absence of bone formation (Fig. 6).

Because fluoride ion is deposited in areas where bone turnover is the greatest, radioactivity levels were high around physeal growth plates (knee, hip) (Fig. 6). Since ROIs were measured in the mid-diaphyseal region of each femur, baseline joint signal uptake did not confound fracture site signal intensity measurements. Net ion uptake around the physeal growth plates was not significantly different between any time points within or between treatment groups (data not shown).

Discussion

Delayed fracture healing and fracture nonunions can lead to significant morbidity for patients, including chronic pain, impaired social functioning, and decreased quality of life [5]. Because orthopedic surgeons have difficulty in identifying those fractures that will ultimately suffer from delayed healing using current imaging modalities, there exists a need for the assessment of bone healing potential to aid in the early surgical intervention for long bone nonunions. In addition, in many challenging situations, diagnosis of fracture nonunions is difficult owing to the quality of plain radiographs, potential artifacts on CT scans, and the subjectivity of patient clinical symptoms [30,66].

PET technology has historically been used to measure skeletal metabolic activity, and our study sought to determine whether PET scans could delineate significant differences between two types of biologic environments. In group I, femoral fractures were created from manual threepoint bending, which exhibited early ^{18}F-fluoride uptake at the ROI 1 week after surgery. The typical 4-week time course of complete bone healing of a well-aligned femoral fracture treated with intramedullary fixation in rats has been reported in previous studies [67,68]. There was significantly greater ^{18}F-fluoride uptake in group I femurs than in group II femurs, in which a spacer was placed to interfere with bony apposition. While it is true that the fractures were created differently in groups I and II, ^{18}F-fluoride ion began localizing to the fracture site soon after surgery in group I animals, revealing high biologic healing potential even 1 week after surgery. Signal intensity on PET scans markedly increased up to the 3-week time point, and then stabilized thereafter. In contrast, PET images in group II revealed significantly less tracer uptake at the fracture site at all time points. ROI SUVs were significantly different between study groups as early as 1 week after surgery ($p \leq 0.005$).

Our data suggest that ^{18}F-fluoride ion PET, which measures in vivo bone turnover, could potentially play an important role in the assessment of longitudinal fracture healing. Early metabolic activity and late bone formation between favorable and unfavorable sites of bony healing were successfully correlated in our study using PET imaging. Current diagnostic methods rely on subjective assessments by orthopedic surgeons and radiologists to determine the fate of bony healing which may occur months later. On the other hand, PET scanning offers a real-time evaluation of metabolic activity, and thus healing potential, of a particular ROI. Moreover, data analysis allows for the quantification of biologic activity, leading to an objective assessment of fracture repair potential.

Biologic factors such as vascular regeneration, bioactive growth factors, and responding cells are critical elements necessary for bone healing; however, no diagnostic method currently exists to assess this potential. Other preliminary studies have successfully utilized ^{18}F-fluoride PET to evaluate the incorporation of bone graft in total hip arthroplasty, bone turnover in Paget's disease, and bone healing potential in women with osteoporosis [31,45,69,70], realizing the advantages of a noninvasive imaging method to assess real-time osteoblastic activity. Consequently, PET scans may ultimately help predict the development of a nonunion at an earlier time point than current routine imaging techniques. For example, if this indication was validated in humans, a PET scan revealing minimal biologic activity of an open tibial fracture site 4–6 weeks after treatment could aid the surgeon in justifying an early bone grafting procedure instead of waiting until a delayed union or bony nonunion had been diagnosed "retrospectively" by plain radiographs.

^{18}F-FDG uptake occurs during localized increased glucose metabolism, which is a direct indicator of tissue inflammation. Although PET imaging using ^{18}F-FDG appears to be effective in many areas of diagnoses, such as primary orthopedic tumors, joint arthroplasty loosening, and prostate cancer metastases [47-50], its utility in the diagnosis of fracture nonunions remains unclear. In our study, inconsistent mean signal intensity was seen in both group I and group II femurs during fracture healing. One explanation for these findings is that the degree of local inflammation is dependent upon a number of variables, including soft tissue healing, bone repair, and muscular insult from postoperative animal activity. Because animals can exhibit different responses to a surgical insult, in vivo glucose uptake by cells with high metabolic activity evidently varies substantially.

There are a number of limitations to this study. Since the study sought to determine the utility of PET scans to detect differences in biologic activity in the course of bone repair, our animal model was designed to compare favorable and suboptimal fracture healing environments. The silastic spacer was necessary to hinder bone formation and form a reliable fracture nonunion model; however, its use may not accurately represent clinical situations where appropriate bony apposition is seen. It stands to reason that one could argue that plain radiographs could be used to successfully identify those femurs that went on to form nonunions in our study. However, the early discernible and quantifiable differences in metabolic activity between study groups demonstrate proof of concept that PET scans using ^{18}F-fluoride ion have potential as a clinical tool in the management of fracture healing. PET imaging offers objective data that may be critical in decision-making when plain radiographs give unclear information.

A second limitation is that this model reflected the biologic activity of an atrophic and not a hypertrophic nonunion. A more stringent preclinical model that could reproducibly distinguish between the formation of bony unions and hypertrophic nonunions, which may also reveal increased signal uptake, would be useful in future studies evaluating the role of PET scans in the assessment of delayed fracture healing. However, to our knowledge, only two published studies have reported the formation of a hypertrophic nonunion from micromotion at the fracture site in an animal model (canine), and none of these nonunions can be reproduced in a consistent manner [71,72].

Another limitation stems from the length of follow-up for both study groups. Because our study was designed to assess the utility of ^{18}F-fluoride ion during fracture healing, the behavior of radioactive tracer uptake after bony union is unknown. Future studies that delineate when ^{18}F-fluoride ion returns to baseline levels after bone repair will be helpful in identifying the relationship between in vivo osteoblastic activity and fracture healing.

To our knowledge, this is the first preclinical study that has utilized PET scan in the evaluation of fracture healing. Our data support the plausibility of PET imaging in the postoperative evaluation of a long bone fracture in the setting of stainless steel hardware, soft tissue dissection, and background radioactivity; however, further study is warranted to determine the indications and imaging techniques for clinical use. PET could eventually be a valuable adjunct to plain radiography during the assessment of fracture healing, but this will have to be determined in a clinical trial. Our plan now is to determine the natural history of PET scan response in healing tibial fractures in humans.

References

1. Heppenstall RB. The present role of bone graft surgery in treating nonunion. Orthop Clin North Am. 1984; 15:113–23. [PubMed: 6364009]
2. Jupiter JB, First K, Gallico GG 3rd, May JW. The role of external fixation in the treatment of posttraumatic osteomyelitis. J Orthop Trauma. 1988; 2:79–93. [PubMed: 3230502]
3. Hulth A. Current concepts of fracture healing. Clin Orthop Relat Res. 1989; 49:265–84. [PubMed: 2684464]
4. Rodriguez-Merchan EC, Forriol F. Nonunion: general principles and experimental data. Clin Orthop Relat Res. 2004; 419:4–12. [PubMed: 15021125]
5. Zlowodzki M, Obremskey WT, Thomison JB, Kregor PJ. Functional outcome after treatment of lower-extremity nonunions. J Trauma. 2005; 58:312–7. [PubMed: 15706193]
6. Bowen CV, Botsford DJ, Hudak PL, Evans PJ. Microsurgical treatment of septic nonunion of the tibia. Quality of life results. Clin Orthop Relat Res. 1996; 332:52–61. [PubMed: 8913145]
7. Sprague S, Bhandari M. An economic evaluation of early versus delayed operative treatment in patients with closed tibial shaft fractures. Arch Orthop Trauma Surg. 2002; 122:315–23. [PubMed: 12136294]
8. Bhandari M, Adili A, Leone J, Lachowski RJ, Kwok DC. Early versus delayed operative management of closed tibial fractures. Clin Orthop Relat Res. 1999; 368:230–9. [PubMed: 10613173]
9. Heckman JD, Sarasohn-Kahn J. The economics of treating tibia fractures. The cost of delayed unions. Bull Hosp Jt Dis. 1997; 56:63–72. [PubMed: 9063607]
10. Ikeda K, Tomita K, Hashimoto F, Morikawa S. Long-term follow-up of vascularized bone grafts for the reconstruction of tibial nonunion: evaluation with computed tomographic scanning. J Trauma. 1992; 32:693–7. [PubMed: 1613828]
11. Savolaine ER, Ebraheim N. Assessment of femoral neck nonunion with multiplanar computed tomography reconstruction. Orthopedics. 2000; 23:713–5. [PubMed: 10917247]
12. Shefelbine SJ, Simon U, Claes L, Gold A, Gabet Y, Bab I, et al. Prediction of fracture callus mechanical properties using micro-CT images and voxel-based finite element analysis. Bone. 2005; 36:480–8. [PubMed: 15777656]
13. Belsole RJ, Hilbelink DR, Llewellyn JA, Dale M, Greene TL, Rayhack JM. Computed analyses of the pathomechanics of scaphoid waist nonunions. J Hand Surg [Am]. 1991; 16:899–906.
14. Kuhlman JE, Fishman EK, Ney DR, Brooker AF Jr, Magid D. Nonunion of acetabular fractures: evaluation with interactive multiplanar CT. J Orthop Trauma. 1989; 3:33–40. [PubMed: 2709202]
15. Kuhlman JE, Fishman EK, Magid D, Scott WW Jr, Brooker AF, Siegelman SS. Fracture nonunion: CT assessment with multi-planar reconstruction. Radiology. 1988; 167:483–8. [PubMed: 3357959]
16. Bhattacharyya T, Bouchard KA, Phadke A, Meigs JB, Kassarjian A, Salamipour H. The accuracy of computed tomography for the diagnosis of tibial nonunion. J Bone Joint Surg Am. 2006; 88:692–7. [PubMed: 16595457]
17. Moed BR, Kim EC, van Holsbeeck M, Schaffler MB, Subramanian S, Bouffard JA, et al. Ultrasound for the early diagnosis of tibial fracture healing after static interlocked nailing without reaming: histologic correlation using a canine model. J Orthop Trauma. 1998; 12:200–5. [PubMed: 9553862]

18. Moed BR, Subramanian S, van Holsbeeck M, Watson JT, Cramer KE, Karges DE, et al. Ultrasound for the early diagnosis of tibial fracture healing after static interlocked nailing without reaming: clinical results. J Orthop Trauma. 1998; 12:206–13. [PubMed: 9553863]
19. Moed BR, Watson JT, Goldschmidt P, van Holsbeeck M. Ultrasound for the early diagnosis of fracture healing after interlocking nailing of the tibia without reaming. Clin Orthop Relat Res. 1995; 310:137–44. [PubMed: 7641429]
20. Derbyshire ND, Simpson AH. A role for ultrasound in limb lengthening. Br J Radiol. 1992; 65:576–80. [PubMed: 1515893]
21. Young JW, Kostrubiak IS, Resnik CS, Paley D. Sonographic evaluation of bone production at the distraction site in Ilizarov limb-lengthening procedures. AJR Am J Roentgenol. 1990; 154:125–8. [PubMed: 2104695]
22. Hirata T, Konishiike T, Kawai A, Sato T, Inoue H. Dynamic magnetic resonance imaging of femoral head perfusion in femoral neck fracture. Clin Orthop Relat Res. 2001; 393:294–301. [PubMed: 11764362]
23. Dailiana ZH, Zachos V, Varitimidis S, Papanagiotou P, Karantanas A, Malizos KN. Scaphoid nonunions treated with vascularised bone grafts: MRI assessment. Eur J Radiol. 2004; 50:217–24. [PubMed: 15145480]
24. De Schrijver F, De Smet L. Isolated fracture of the capitate: the value of MRI in diagnosis and follow up. Acta Orthop Belg. 2002; 68:310–5. [PubMed: 12152383]
25. Lee C, Dorcil J, Radomisli TE. Nonunion of the spine: a review. Clin Orthop Relat Res. 2004; 419:71–5. [PubMed: 15021134]
26. Kuschner SH, Lane CS, Brien WW, Gellman H. Scaphoid fractures and scaphoid nonunion. Diagnosis and treatment. Orthop Rev. 1994; 23:861–71. [PubMed: 7854839]
27. Rayan GM. Occult wrist pain due to capitate nonunion. South Med J. 1994; 87:402–4. [PubMed: 8134866]
28. Schelstraete K, Daneels F, Obrie E. Technetium-99m-diphosphonate, gallium-67 and labeled leukocyte scanning techniques in tibial nonunion. Acta Orthop Belg. 1992; 58(Suppl 1):168–72. [PubMed: 1456000]
29. O'Reilly RJ, Cook DJ, Gaffney RD, Angel KR, Paterson DC. Can serial scintigraphic studies detect delayed fracture union in man? Clin Orthop Relat Res. 1981; 160:227–32. [PubMed: 6456857]
30. Ebraheim NA, Savolaine ER, Patel A, Skie M, Jackson WT. Assessment of tibial fracture union by 35–45 degrees internal oblique radiographs. J Orthop Trauma. 1991; 5:349–50. [PubMed: 1941319]
31. Sorensen J, Ullmark G, Langstrom B, Nilsson O. Rapid bone and blood flow formation in impacted morselized allografts: positron emission tomography (PET) studies on allografts in 5 femoral component revisions of total hip arthroplasty. Acta Orthop Scand. 2003; 74:633–43. [PubMed: 14763691]
32. Blau M, Nagler W, Bender MA. Fluorine-18: a new isotope for bone scanning. J Nucl Med. 1962; 3:332–4. [PubMed: 13869926]
33. Narita N, Kato K, Nakagaki H, Ohno N, Kameyama Y, Weatherell JA. Distribution of fluoride concentration in the rat's bone. Calcif Tissue Int. 1990; 46:200–4. [PubMed: 2106380]
34. Toegel S, Hoffmann O, Wadsak W, Ettlinger D, Mien LK, Wiesner K, et al. Uptake of bone-seekers is solely associated with mineralisation! A study with ^{99m}Tc-MDP, ^{153}Sm-EDTMP and ^{18}F-fluoride on osteoblasts. Eur J Nucl Med Mol Imaging. 2006; 33:491–4. [PubMed: 16416330]
35. Blau M, Ganatra R, Bender MA. ^{18}F-fluoride for bone imaging. Semin Nucl Med. 1972; 2:31–7. [PubMed: 5059349]
36. Reeve J, Arlot M, Wootton R, Edouard C, Tellez M, Hesp R, et al. Skeletal blood flow, iliac histomorphometry, and strontium kinetics in osteoporosis: a relationship between blood flow and corrected apposition rate. J Clin Endocrinol Metab. 1988; 66:1124–31. [PubMed: 3372678]
37. Hawkins RA, Choi Y, Huang SC, Hoh CK, Dahlbom M, Schiepers C, et al. Evaluation of the skeletal kinetics of fluorine-18-fluoride ion with PET. J Nucl Med. 1992; 33:633–42. [PubMed: 1569473]

38. Schiepers C, Nuyts J, Bormans G, Dequeker J, Bouillon R, Mortelmans L, et al. Fluoride kinetics of the axial skeleton measured in vivo with fluorine-18-fluoride PET. J Nucl Med. 1997; 38:1970–6. [PubMed: 9430479]
39. Cook GJ, Fogelman I. The role of positron emission tomography in the management of bone metastases. Cancer. 2000; 88(12 Suppl):2927–33. [PubMed: 10898336]
40. Blake GM, Park-Holohan SJ, Cook GJ, Fogelman I. Quantitative studies of bone with the use of ^{18}F-fluoride and ^{99m}Tc-methylene diphosphonate. Semin Nucl Med. 2001; 31:28–49. [PubMed: 11200203]
41. Schwartz Z, Shani J, Soskolne WA, Touma H, Amir D, Sela J. Uptake and biodistribution of technetium-99m-MD32P during rat tibial bone repair. J Nucl Med. 1993; 34:104–8. [PubMed: 8418249]
42. Berger F, Lee YP, Loening AM, Chatziioannou A, Freedland SJ, Leahy R, et al. Whole-body skeletal imaging in mice utilizing microPET: optimization of reproducibility and applications in animal models of bone disease. Eur J Nucl Med Mol Imaging. 2002; 29:1225–36. [PubMed: 12418463]
43. Even-Sapir E, Metser U, Flusser G, Zuriel L, Kollender Y, Lerman H, et al. Assessment of malignant skeletal disease: initial experience with ^{18}F-fluoride PET/CT and comparison between ^{18}F-fluoride PET and ^{18}F-fluoride PET/CT. J Nucl Med. 2004; 45:272–8. [PubMed: 14960647]
44. Frost ML, Fogelman I, Blake GM, Marsden PK, Cook G Jr. Dissociation between global markers of bone formation and direct measurement of spinal bone formation in osteoporosis. J Bone Miner Res. 2004; 19:1797–804. [PubMed: 15476579]
45. Cook GJ, Blake GM, Marsden PK, Cronin B, Fogelman I. Quantification of skeletal kinetic indices in Paget's disease using dynamic ^{18}F-fluoride positron emission tomography. J Bone Miner Res. 2002; 17:854–9. [PubMed: 12009016]
46. Pakos EE, Fotopoulos AD, Ioannidis JP. ^{18}F-FDG PET for evaluation of bone marrow infiltration in staging of lymphoma: a meta-analysis. J Nucl Med. 2005; 46:958–63. [PubMed: 15937306]
47. Hsu, W.; Feeley, B.; Krenek, L.; Gamradt, S.; Stout, D.; Chatziioannou, A., et al. The characterization of osteolytic and osteoblastic lesions in a prostate cancer mouse model with the use of ^{18}F-FDG and ^{18}F-fluoride PET/CT scans; Transactions of the 51st Annual Meeting of the Orthopaedic Research Society; Washington DC. 2005;
48. Lee FY, Yu J, Chang SS, Fawwaz R, Parisien MV. Diagnostic value and limitations of fluorine-18 fluorodeoxyglucose positron emission tomography for cartilaginous tumors of bone. J Bone Joint Surg Am. 2004; 86-A:2677–85. [PubMed: 15590853]
49. Mumme T, Reinartz P, Alfer J, Muller-Rath R, Buell U, Wirtz DC. Diagnostic values of positron emission tomography versus triple-phase bone scan in hip arthroplasty loosening. Arch Orthop Trauma Surg. 2005; 125:322–9. [PubMed: 15821896]
50. Strauss LG, Dimitrakopoulou-Strauss A, Koczan D, Bernd L, Haberkorn U, Ewerbeck V, et al. ^{18}F-FDG kinetics and gene expression in giant cell tumors. J Nucl Med. 2004; 45:1528–35. [PubMed: 15347720]
51. Eary JF, O'Sullivan F, Powitan Y, Chandhury KR, Vernon C, Bruckner JD, et al. Sarcoma tumor FDG uptake measured by PET and patient outcome: a retrospective analysis. Eur J Nucl Med Mol Imaging. 2002; 29:1149–54. [PubMed: 12192559]
52. Hawkins DS, Schuetze SM, Butrynski JE, Rajendran JG, Vernon CB, Conrad EU 3rd, et al. [^{18}F]Fluorodeoxyglucose positron emission tomography predicts outcome for Ewing sarcoma family of tumors. J Clin Oncol. 2005; 23:8828–34. [PubMed: 16314643]
53. O'Sullivan F, Roy S, O'Sullivan J, Vernon C, Eary J. Incorporation of tumor shape into an assessment of spatial heterogeneity for human sarcomas imaged with FDG-PET. Biostatistics. 2005; 6:293–301. [PubMed: 15772107]
54. Schuetze SM, Rubin BP, Vernon C, Hawkins DS, Bruckner JD, Conrad EU 3rd, et al. Use of positron emission tomography in localized extremity soft tissue sarcoma treated with neoadjuvant chemotherapy. Cancer. 2005; 103:339–48. [PubMed: 15578712]
55. Shields AF, Mankoff DA, Link JM, Graham MM, Eary JF, Kozawa SM, et al. Carbon-11-thymidine and FDG to measure therapy response. J Nucl Med. 1998; 39:1757–62. [PubMed: 9776283]

56. Blokhuis TJ, Patka P, Bakker FC, Haarman HJ, van Lingen A, Roos JC, et al. Quantitative assessment of fracture healing using positron emission tomography. Eur J Nucl Med Mol Imaging. 2003; 30:329–30. [PubMed: 12645528]
57. Piert M, Zittel TT, Becker GA, Jahn M, Stahlschmidt A, Maier G, et al. Assessment of porcine bone metabolism by dynamic ^{18}F-fluoride ion PET: correlation with bone histomorphometry. J Nucl Med. 2001; 42:1091–100. [PubMed: 11438633]
58. Messa C, Goodman WG, Hoh CK, Choi Y, Nissenson AR, Salusky IB, et al. Bone metabolic activity measured with positron emission tomography and [^{18}F]fluoride ion in renal osteodystrophy: correlation with bone histomorphometry. J Clin Endocrinol Metab. 1993; 77:949–55. [PubMed: 8408470]
59. Peterson B, Zhang J, Iglesias R, Kabo M, Hedrick M, Benhaim P, et al. Healing of critically sized femoral defects, using genetically modified mesenchymal stem cells from human adipose tissue. Tissue Eng. 2005; 11:120–9. [PubMed: 15738667]
60. Wieland, B.; Bida, G.; Padgett, H.; Go, H. Current status of CTI target systems for the production of PET radiochemicals; Proceedings of the 3rd Workshop on Targetry and Target Chemistry; 1989;
61. Hamacher K, Coenen HH, Stocklin G. Efficient stereospecific synthesis of no-carrier-added 2-[^{18}F]-fluoro-2-deoxy-D-glucose using aminopolyether supported nucleophilic substitution. J Nucl Med. 1986; 27:235–8. [PubMed: 3712040]
62. Stout D, Chow P, Gustilo A, Grubwieser S, Chatziioannou A. Multimodality isolated bed system for mouse imaging experiments. Molecular Imaging and Biology. 2003; 5:128–29.
63. Tai YC, Ruangma A, Rowland D, Siegel S, Newport DF, Chow PL, et al. Performance evaluation of the microPET focus: a third-generation microPET scanner dedicated to animal imaging. J Nucl Med. 2005; 46:455–63. [PubMed: 15750159]
64. Chatziioannou A, Qi J, Moore A, Annala A, Nguyen K, Leahy R, et al. Comparison of 3-D maximum a posteriori and filtered backprojection algorithms for high-resolution animal imaging with microPET. IEEE Trans Med Imaging. 2000; 19:507–12. [PubMed: 11021693]
65. Loening AM, Gambhir SS. AMIDE: a free software tool for multimodality medical image analysis. Mol Imaging. 2003; 2:131–7. [PubMed: 14649056]
66. Whelan DB, Bhandari M, McKee MD, Guyatt GH, Kreder HJ, Stephen D, et al. Interobserver and intraobserver variation in the assessment of the healing of tibial fractures after intramedullary fixation. J Bone Joint Surg Br. 2002; 84:15–8. [PubMed: 11837825]
67. Kokubu T, Hak DJ, Hazelwood SJ, Reddi AH. Development of an atrophic nonunion model and comparison to a closed healing fracture in rat femur. J Orthop Res. 2003; 21:503–10. [PubMed: 12706024]
68. Einhorn TA, Majeska RJ, Mohaideen A, Kagel EM, Bouxsein ML, Turek TJ, et al. A single percutaneous injection of recombinant human bone morphogenetic protein-2 accelerates fracture repair. J Bone Joint Surg Am. 2003; 85-A:1425–35. [PubMed: 12925621]
69. Frost ML, Cook GJ, Blake GM, Marsden PK, Benatar NA, Fogelman I. A prospective study of risedronate on regional bone metabolism and blood flow at the lumbar spine measured by ^{18}F-fluoride positron emission tomography. J Bone Miner Res. 2003; 18:2215–22. [PubMed: 14672357]
70. Brenner W, Vernon C, Conrad EU, Eary JF. Assessment of the metabolic activity of bone grafts with ^{18}F-fluoride PET. Eur J Nucl Med Mol Imaging. 2004; 31:1291–8. [PubMed: 15197502]
71. dos Santos Neto FL, Volpon JB. Experimental nonunion in dogs. Clin Orthop Relat Res. 1984; 187:260–71. [PubMed: 6086197]
72. Volpon JB. Nonunion using a canine model. Arch Orthop Trauma Surg. 1994; 113:312–7. [PubMed: 7833207]

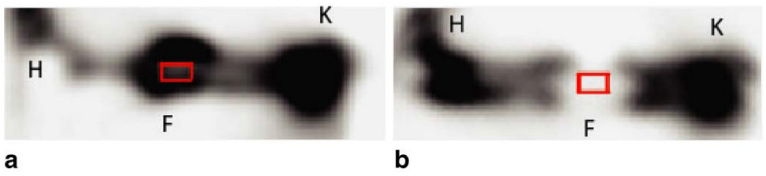

Fig. 1.
^{18}F-fluoride ion PET images of group I (**a**) and group II (**b**) femurs demonstrating standardization of the ROI (*red box*). Successive coronal images were then reconstructed with a 4-mm depth to approximate the fracture site seen on plain radiographs. Volumes of interest were then used for data calculations. *K* knee, *F* fracture site, *H* hip

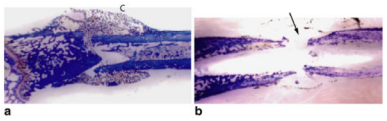

Fig. 2.

Histological longitudinal sections, stained with toluidine blue, of representative group I (**a**) and group II (**b**) femurs harvested 4 weeks after surgical treatment. Abundant bridging callus formation (*C*) indicative of healing is seen in the group I femur, while fibrous tissue and minimal new bone formation are seen at the operative site (*arrow*) for femurs in group II

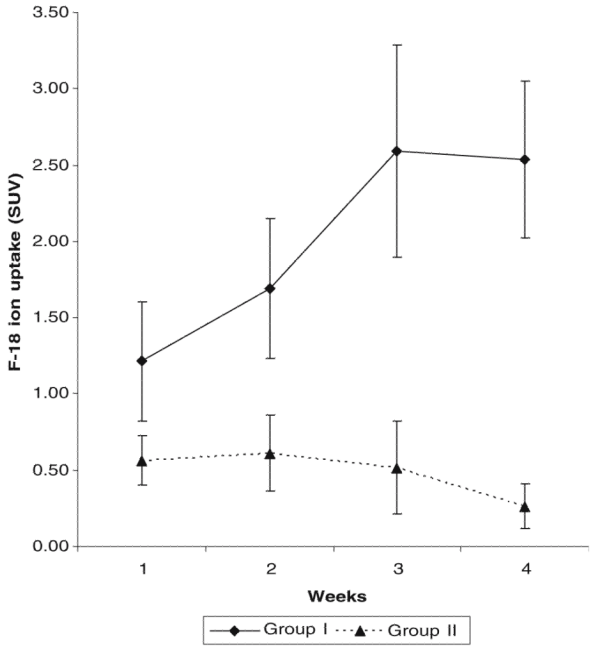

Week	Group I	Group II	p-value
1	1.21	0.56	0.0053
2	1.69	0.61	0.00012
3	2.59	0.52	0.000019
4	2.54	0.26	0.000002

Fig. 3.

SUV in group I and group II femurs at weekly time points using ^{18}F-fluoride ion. ROIs in group I steadily increased in mean signal intensity until 3 weeks, then leveled off, while in group II there was minimal tracer uptake at all time points. Statistically significant differences in tracer uptake were seen at all time points

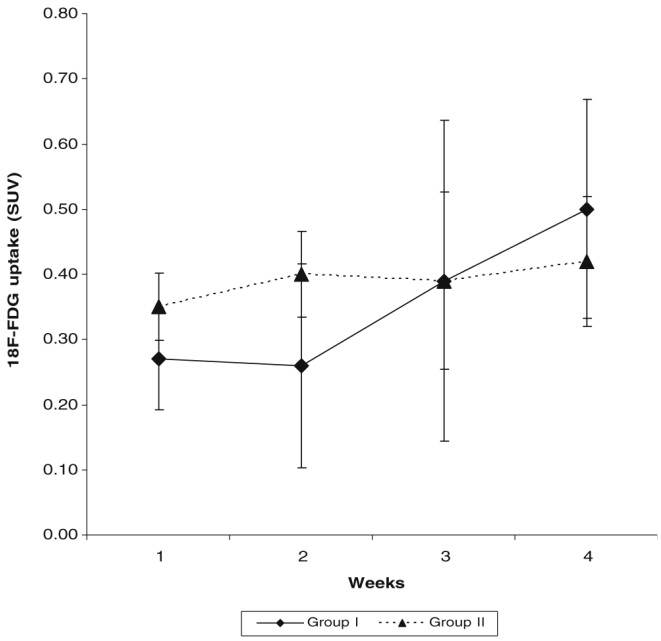

Week	Group I	Group II	p-value
1	0.27	0.35	0.10
2	0.26	0.40	0.12
3	0.39	0.39	0.92
4	0.50	0.42	0.33

Fig. 4.

SUVs in group I and group II femurs at weekly time points using ^{18}F-FDG. Localized tracer uptake was seen as early as 1 week after surgery with minimal increasing intensity at each time point in both groups. There were no statistically significant differences in mean signal intensity between or within groups at any time point

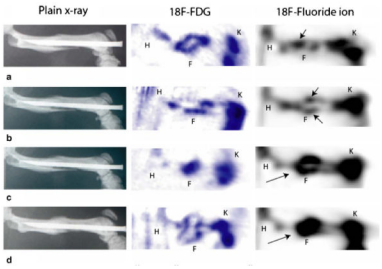

Fig. 5.

Plain AP radiograph and corresponding ^{18}F-FDG and ^{18}F-fluoride PET images of a femur from group I at 1 week (**a**), 2 weeks (**b**), 3 weeks (**c**), and 4 weeks (**d**) post fracture. While callus formation can be identified on plain radiographs as early as 2 weeks (**b**), PET scan images using ^{18}F-fluoride ion show increasing biologic activity (*arrows*) in the union site during fracture repair at successive time points. In contrast, no significant differences were seen in ^{18}F-FDG tracer uptake at any time point. *K* knee, *F* fracture site, *H* hip

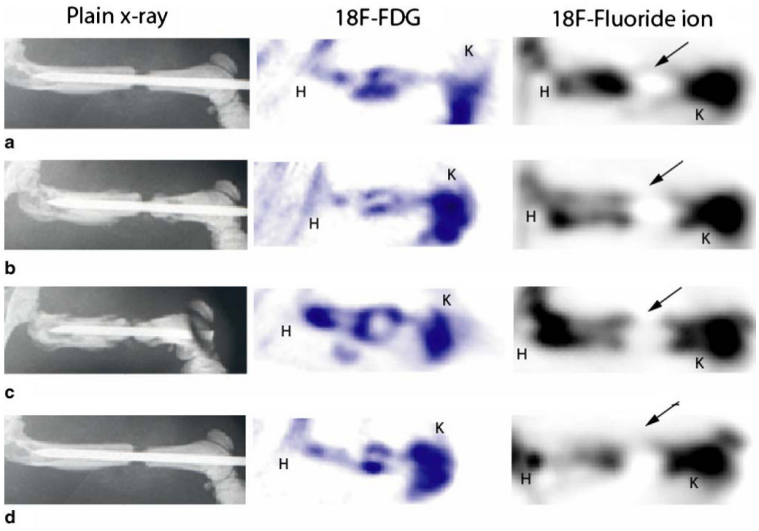

Fig. 6.

Plain AP radiograph and corresponding ^{18}F-FDG and ^{18}F-fluoride PET scan images of a femur from group II at 1 week (**a**), 2 weeks (**b**), 3 weeks (**c**), and 4 weeks (**d**) after surgery. Plain radiographs reveal the maintenance of a bony gap and no bridging bone at the surgical site even 4 weeks after surgery (**d**). Corresponding PET images using ^{18}F-fluoride show tracer uptake extending into the fracture site from the bony ends; however, signal intensity is minimal at all time points, revealing poor biologic healing potential. Despite the absence of bone formation within the fracture site, significant localized uptake of ^{18}F-FDG is seen at all time points. *K* knee, *arrows* nonunion site, *H* hip